AGU PUBLICATIONS

JGR

Journal of Geophysical Research: Biogeosciences

RESEARCH ARTICLE
10.1002/2017JG004370

Key Points:
- Median model efficiency coefficients from validation of four semiempirical PAR partitioning models applied to 58 sites ranged from 0.62 to 0.69
- We present a simple new universal PAR partitioning model which improved model accuracy by 4-10% and lowered intersite accuracy variability
- Site-optimized PAR partitioning model coefficients improved accuracy over universal models and suggests the potential for regional coefficient development

Supporting Information:
- Supporting Information S1
- Data Set S1

Correspondence to:
A. J. Oliphant,
andrewo@sfsu.edu

Citation:
Oliphant, A. J., & Stoy, P. C. (2018). An evaluation of semiempirical models for partitioning photosynthetically active radiation into diffuse and direct beam components. *Journal of Geophysical Research: Biogeosciences*, *123*, 889–901. https://doi.org/10.1002/2017JG004370

Received 18 DEC 2017
Accepted 7 FEB 2018
Accepted article online 13 FEB 2018
Published online 11 MAR 2018

An Evaluation of Semiempirical Models for Partitioning Photosynthetically Active Radiation Into Diffuse and Direct Beam Components

Andrew J. Oliphant[1] **and Paul C. Stoy**[2]

[1]Department of Geography & Environment, San Francisco State University, San Francisco, CA, USA, [2]Department of Land Resources and Environmental Sciences, Montana State University, Bozeman, MT, USA

Abstract Photosynthesis is more efficient under diffuse than direct beam photosynthetically active radiation (PAR) per unit PAR, but diffuse PAR is infrequently measured at research sites. We examine four commonly used semiempirical models (Erbs et al., 1982, https://doi.org/10.1016/0038-092X(82)90302-4; Gu et al., 1999, https://doi.org/10.1029/1999JD901068; Roderick, 1999, https://doi.org/10.1016/S0168-1923(99)00028-3; Weiss & Norman, 1985, https://doi.org/10.1016/0168-1923(85)90020-6) that partition PAR into diffuse and direct beam components based on the negative relationship between atmospheric transparency and scattering of PAR. Radiation observations at 58 sites (140 site years) from the La Thuille FLUXNET data set were used for model validation and coefficient testing. All four models did a reasonable job of predicting the diffuse fraction of PAR (ϕ) at the 30 min timescale, with site median r^2 values ranging between 0.85 and 0.87, model efficiency coefficients (MECs) between 0.62 and 0.69, and regression slopes within 10% of unity. Model residuals were not strongly correlated with astronomical or standard meteorological variables. We conclude that the Roderick (1999, https://doi.org/10.1016/S0168-1923(99)00028-3) and Gu et al. (1999, https://doi.org/10.1029/1999JD901068) models performed better overall than the two older models. Using the basic form of these models, the data set was used to find both individual site and universal model coefficients that optimized predictive accuracy. A new universal form of the model is presented in section 5 that increased site median MEC to 0.73. Site-specific model coefficients increased median MEC further to 0.78, indicating usefulness of local/regional training of coefficients to capture the local distributions of aerosols and cloud types.

1. Introduction

Solar radiation (K) is the principal driver of the planetary energy balance and photosynthesis. In order to fully understand its role in the Earth system, it is necessary to distinguish the magnitude of global radiation (K_G) arriving in its direct beam (K_S) *versus* diffuse beam (K_D) forms. Different relative levels of these forms result in different irradiance patterns within plant canopies (Norman & Welles, 1983) and across heterogeneous terrain (Oliphant et al., 2003, 2006) (see Table 1 for a list of symbols). For example, global photosynthetically active radiation (PAR_G)—a spectral subset of K_G—is more efficient for canopy photosynthesis under conditions of diffuse beam PAR (PAR_D) than direct beam PAR (PAR_S) per unit PAR (Alton, 2008; Cheng et al., 2015, 2016; Gu et al., 1999, 2002; Keppel-Aleks & Washenfelder, 2016; Mercado et al., 2009; Oliphant et al., 2011). Furthermore, the ratio of K_D to K_G has been found to lower the Bowen ratio (the ratio of sensible to latent heat flux) in a number of ecosystems (Steiner et al., 2013) and is important for the spatial distribution of net radiation in complex natural and urban terrain (e.g., Lindberg et al., 2014; Oliphant et al., 2003). Despite their importance, neither K_D nor PAR_D are commonly measured at standard meteorological stations or eddy covariance flux towers, making it unclear how trends in these variables have impacted the flux of trace gases and energy at the ecosystem scale. Models of PAR_D and PAR_S as well as K_D and K_S have been developed and used for studies of the surface-atmosphere exchange of mass and energy (Alton, 2008; Goudriaan & Van Laar, 2012; Gu et al., 1999; Leuning et al., 1995) but have rarely been compared against each other, leaving it unclear which model performs best across a range of atmospheric and solar conditions (Lee et al., 2018), and which may be best for global synthesis or biophysical modeling studies.

Models for partitioning K_D and K_S using observations of K_G use physical or semiempirical approaches, that is, those that use simple functions to model atmospheric transmissivity (τ). Physical models such as Nunez (1980) or Alados et al. (2002) explicitly resolve wavelength-specific diffuse and direct beam irradiance that result from scattering in

Table 1
A list of Abbreviations

Abbreviation	Definition	Units
A_0	Intercept parameter of the ϕ_K relationship	—
A_1	Slope parameter of the ϕ_K relationship	—
β	Solar elevation angle	degrees
ϕ	Diffuse fraction of PAR (PAR_D/PAR_G)	—
ϕ_K	Diffuse fraction of solar radiation (K_D/K_G)	—
ϕ_0	Lower inflection point value for ϕ	—
ϕ_1	Upper inflection point value for ϕ	—
γ	Latitude	degrees
φ	PAR_S fraction	—
φ_{pot}	Equivalent PAR_S fraction for a clear-sky case	—
K	Solar radiation	W m^{-2}
K_G	Global solar radiation	W m^{-2}
K_S	Direct beam solar radiation	W m^{-2}
K_D	Diffuse beam solar radiation	W m^{-2}
K_{Ex}	Extraterrestrial solar radiation	W m^{-2}
MEC	Model efficiency coefficient (Nash & Sutcliffe, 1970)	—
m	Modeled data (used as subscript)	
o	Observed data (used as subscript)	
PAR_G	Photosynthetically active radiation (global)	μmol m^{-2} s^{-1}
PAR_D	Diffuse beam PAR	μmol m^{-2} s^{-1}
PAR_S	Direct beam PAR	μmol m^{-2} s^{-1}
q	Diffuse fraction-transmissivity ratio $q=(\phi_K/\tau)$	—
SD	Standard deviation	
t	Time (30 min periods)	0.5 h
τ	Atmospheric transmissivity (K_G/K_{Ex})	—
τ_0	Lower inflection point value for τ	—
τ_1	Upper inflection point value for τ	—
x	Exponent coefficient used for line curvature	0.5–2

the atmosphere by ozone, aerosols, and clouds (McCartney, 1976). These models require considerable information about atmospheric conditions and constituents, which can be difficult to obtain and are not widely available in the historical or even the modern data record. Liu and Jordan (1960) proposed an alternative semiempirical approach to model τ that has been widely used and modified (e.g., Alton, 2008; Erbs et al., 1982; Roderick, 1999; Spitters et al., 1986; Weiss & Norman, 1985; see section 2.2). The attraction of the semiempirical approach is that no a priori knowledge is required of atmospheric conditions and constituents, and the K_G and/or PAR_G observations required by the models are some of the more commonly measured variables in standard meteorological and micrometeorological measurement systems.

Here we report the results of a comparison of four commonly used semiempirical models for partitioning PAR_G into PAR_D and PAR_S across a range of ecosystems, climates, and latitudes. Our objectives are to compare model performance at the 30 min timescale, assess model residuals, explore approaches to improve model performance, and to discuss implications of applying modeled PAR_D to research in Biogeoscience, particularly studies of ecosystem-atmosphere CO_2 exchanges.

2. Materials and Methods

We first discuss the theory underlying semiempirical models for partitioning direct and diffuse radiation followed by definition of the models explored here. We then describe the PAR_D and PAR_G observations from the La Thuile FLUXNET database (Baldocchi et al., 2001) that were used to validate model performance and to train model development.

2.1. Theory

The approach taken by semiempirical models to determine the diffuse fraction of PAR ($\phi = PAR_D/PAR_G$) is based on its negative relation with atmospheric transmissivity of solar radiation (τ),

$$\varnothing = A_0 + A_1\tau, \tag{1}$$

where A_0 and A_1 are offset and slope coefficients determined by regression and τ is a form of optical transmissivity that maintains the effect of atmospheric path length on transmission, referred to by Gu et al. (1999) and others as the "clearness index,"

$$\tau = \frac{K_G}{K_{Ex}}, \tag{2}$$

where K_{Ex} is solar radiation at the top of the atmosphere. Modeling K_{Ex} is fairly simple and only requires knowledge of one's location on Earth's surface and time (e.g., Whiteman & Allwine, 1986). K_G and PAR_G are measured using upward pointing pyranometers or quantum sensors mounted above the surface with an unobstructed sky view (see section 2.3).

Equation (1) is only valid for τ values above about 0.3. Below this value, the model inflects to a flat line representing the maximum ϕ value, usually between 0.9 and 0.95 (e.g., Roderick, 1999). This occurs mostly under cloudy conditions, and the inflection point represents a threshold in optical transmissivity, below which almost all incident PAR arrives in diffuse form. Many previous studies have included a second inflection point at an upper threshold of τ, above which ϕ remains nears its minimum. This occurs under the clearest sky conditions and lowest zenith angles. In reality considerable variability exists at high levels of τ and the inflection point is less obvious than when ϕ saturates at low τ levels. The general relationship described above is illustrated by data shown in Figure 2a.

2.2. Semiempirical Models for Partitioning Direct and Diffuse Shortwave Radiation

The four models chosen for analysis are commonly cited semiempirical approaches that use some form of the relationship described in equation (1).

1. Erbs et al. (1982) presented a simple method for calculating the diffuse fraction of the full solar spectrum ($\phi_K = K_D/K_G$) using τ. Despite modeling the diffuse fraction of the full solar spectrum rather than the photosynthetically active portion, this relation has been widely used in plant biophysical models for partitioning of PAR_G (e.g., Goudriaan & Van Laar, 2012; Leuning et al., 1995):

$$\text{for} \tau < 0.22, \quad \phi_K = 1.0 - 0.09\tau, \tag{3}$$

$$\text{for } 0.22 \le \tau \le 0.80, \quad \phi_K = 0.9511 - 0.1604\tau + 4.388\tau^2 - 16.638\tau^3 + 12.336\tau^4 \tag{4}$$

$$\text{for} \tau > 0.80, \quad \phi_K = 0.16. \tag{5}$$

2. Reindl et al. (1990) examined a variety of potential atmospheric and geometric controls on ϕ_K. The four significant predictors in order of significance were τ, solar elevation angle (β), air temperature, and relative humidity (RH). Gu et al. (1999) simplified this to the two strongest predictors to derive the diffuse partitioning of full spectrum solar radiation based on τ and β:

$$\text{for } \tau \le 0.3, \phi_K = \tau[1.02 - 0.254\tau + 0.0123 \sin\beta], \tag{6}$$

$$\text{for } 0.3 < \tau < 0.78, \phi_K = \tau[1.4 - 1.749\tau + 0.177 \sin\beta], \tag{7}$$

$$\text{for } \tau \ge 0.78, \phi_K = \tau[0.486\tau - 0.182 \sin\beta], \tag{8}$$

where β is the solar elevation angle. The resulting model is also constrained between the limits of 0.1 and 0.96 since even the clearest skies produce at least 10% scattered light and even the most overcast skies produce a small portion of irradiance directly from the direction of the Sun. Gu et al. (1999) combined this with a modification to derive the diffuse fraction of PAR ($\phi = PAR_D/PAR_G$) using the approach of Spitters et al. (1986):

$$\phi = \frac{[1 + 0.3(1 - q^2)]q}{1 + (1 - q^2)\cos^2(90 - \beta)\cos^3\beta}, \tag{9}$$

where

$$q = (\phi_K/\tau). \tag{10}$$

3. Weiss and Norman (1985) first modeled clear-sky potential PAR_D, and PAR_S using a simple Beer's law approach. From this, the clear-sky potential direct beam fraction of PAR (φ_{pot}) was derived from modeled clear-sky PAR_S/PAR_G. φ_{pot} was then modified to determine the actual direct beam fraction (φ) using τ,

$$\varphi = \varphi_{pot}\left[1 - \left(\frac{0.9 - \tau}{0.7}\right)^{2/3}\right]. \tag{11}$$

From this, ϕ was determined by $\phi = 1 - \varphi$. For the Weiss and Norman (1985) model we also added upper and lower ϕ constraints of 0.96 and 0.05, respectively, following Gu et al. (1999).

4. Roderick (1999) found a simplified linear model that could be universally applied across 25 measurement sites at a range of latitudes in Australia and Antarctica for daily and monthly time steps. This approach focused on identifying the optimal inflection points in the same simplified relationship described originally by Erbs et al. (1982). The lower inflection point for ϕ (ϕ_0) was 0.05 and the upper inflection point (ϕ_1) was 0.96. The lower inflection point for τ (τ_0), was found to be 0.26, and the upper inflection point (τ_1) was found to correlate with latitude (γ), so

$$\text{for} \tau < 0.26, \phi = \phi_0 = 0.96 \tag{12}$$

$$\text{for} \tau_0 < \tau > \tau_1, \quad \phi = A_0 + A_1\tau, \tag{13}$$

Table 2
The Site Abbreviation and Location of Sites in the La Thuille FLUXNET Database With Partitioned Direct and Diffuse Photosynthetically Active Radiation Measurements Explored in the Present Analysis

Site ID	Latitude (decimal degrees)	Longitude (decimal degrees)	Elevation (asl, m)	Reference
AT-Neu	47.11667	11.3175	970	Wohlfahrt et al. (2008)
AU-How	−12.4943	131.152	133	Hutley et al. (2000)
BE-Bra	51.3092	4.52056	16	de Pury & Ceulemans (1997)
BE-Lon	50.5522	4.74494	167	Moureaux et al. (2006)
BE-Vie	50.3055	5.99683	450	Aubinet et al. (2001)
CZ-Bk1	49.503	18.538	908	Marek et al. (2011)
CZ-Bk2	49.495	18.545	855	Marek et al. (2011)
DE-Geb	51.1001	10.9143	162	Anthoni, Freibauer, et al. (2004)
DE-Hai	51.0793	10.452	430	Knohl et al. (2003)
DE-Meh	51.2753	10.6555	286	Don et al. (2009)
DE-Tha	50.9636	13.5669	380	Bernhofer et al. (2003)
DE-Wet	50.4535	11.4575	785	Anthoni, Knohl, et al. (2004)
DK-Fou	56.4842	9.58722	51	Soegaard et al. (2003)
DK-Lva	55.6833	12.0833	15	Soussana et al. (2007)
DK-Sor	55.4869	11.6458	40	Pilegaard et al. (2001)
ES-ES2	39.2755	−0.31522	10	Carvalhais et al. (2010)
ES-LMa	39.9415	−5.77336	260	Carvalhais et al. (2010)
ES-VDA	42.1522	1.4485	1,770	Gilmanov et al. (2007)
FI-Hyy	61.8474	24.2948	181	Suni et al. (2003)
FI-Kaa	69.1407	27.295	155	Aurela et al. (2002)
FR-Aur	43.5494	1.10778	793	Béziat et al. (2009)
FR-Lam	43.4933	1.23722	181	Béziat et al. (2009)
FR-Fon	48.4763	2.7801	90	Davi et al. (2006)
FR-Gri	48.844	1.95243	125	Laville et al. (1999)
FR-Hes	48.6742	7.06462	300	Granier et al. (2000)
FR-LBr	44.7171	−0.7693	61	Berbigier et al. (2001)
FR-Pue	43.7414	3.59583	270	Rambal et al. (2004)
IE-Ca1	52.8588	−6.91814	50	Black et al. (2006)
IT-Amp	41.9041	13.6052	884	Wohlfahrt et al. (2008)
IT-BCi	40.5238	14.9574	20	Reichstein et al. (2003)
IT-Cas	45.06285	8.668539	294	Skiba et al. (2009)
IT-Col	41.8494	13.5881	1,550	Valentini et al. (1996)
IT-Cpz	41.7052	12.3761	68	Tirone et al. (2003)
IT-Lav	45.9553	11.2812	1,353	Cescatti and Marcolla (2004)
IT-MBo	46.0156	11.0467	1,550	Marcolla et al. (2011)
IT-PT1	45.2009	9.06104	60	Migliavacca et al. (2009)
IT-Ren	46.5878	11.4347	1,730	Marcolla et al. (2005)
IT-Ro1	42.4081	11.93	235	Rey et al. (2002)
IT-Ro2	42.3903	11.9209	224	Tedeschi et al. (2006)
IT-SRo	43.72786	10.28444	4	Chiesi et al. (2005)
NL-Ca1	51.971	4.927	0.7	Gilmanov et al. (2007)
NL-Lan	51.9536	4.9029	−6	Moors et al. (2010)
NL-Loo	52.1679	5.74396	25	Dolman et al. (2002)
NL-Lut	53.3989	6.356	−1	Moors et al. (2010)
NL-Mol	51.650	4.6390	−1	Moors et al. (2010)
PL-Wet	52.7622	16.3094	54	Chojnicki et al. (2007)
PT-Mi2	38.4765	−8.02455	190	Pereira et al. (2007)
SE-Nor	60.0865	17.4795	43	Lagergren et al. (2005)
UK-EBu	55.866	−3.20578	190	Famulari et al. (2004)
US-Bar	44.065	−71.288	272	Richardson et al. (2007)
US-Me1	44.5794	−121.5	896	Law et al. (2001)
US-M	39.3231	−86.4131	275	Schmid et al. (2000)
US-Ne1	41.1651	−96.4766	361	Verma et al. (2005)
US-Ne2	41.1649	−96.4701	362	Verma et al. (2005)
US-Ne3	41.1797	−96.4397	363	Verma et al. (2005)
US-Var	38.4133	−120.9507	129	Ma et al. (2007)
US-WCr	45.8059	−90.0799	520	Cook et al. (2004)
VU-Coc	−15.443	167.19	80	Roupsard et al. (2006)

Note. Elevation data that were missing were retrieved from a digital elevation model using geographic coordinates.

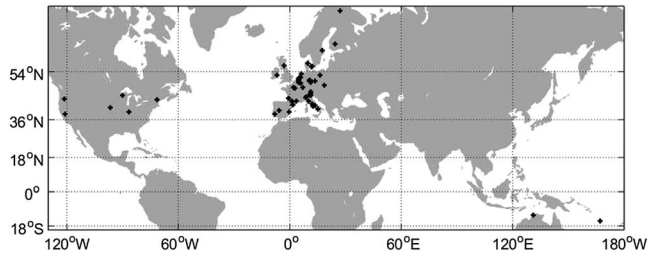

Figure 1. A map of sites in the La Thuille database with partitioned direct and diffuse photosynthetically active radiation measurements used in the analysis presented (see Table 1 for site list).

$$\text{where } A_1 = \frac{\phi_1 - \phi_0}{\tau_1 - \tau_0} \quad \text{and} \quad A_0 = \phi_1 - A_1\tau_1, \tag{14}$$

$$\text{where } \tau_1 = 0.8 + 0.0017\gamma + 0.000044\gamma^2, \text{and} \tag{15}$$

$$\text{for} \tau > \tau_1, \phi = 0.05. \tag{16}$$

The approach of Roderick (1999) was further simplified by Alton (2008) and applied at 30 min time steps using ϕ_0 = 0.1 and ϕ_1 = 0.95, τ_0 = 0.28 and τ_1 = 0.75. By fixing all four points, the single resulting linear function for $\tau_0 < \tau < \tau_1$ was ϕ = 1.45–1.81τ.

2.3. Observations of Direct and Diffuse Photosynthetically Active Radiation

Data were extracted from the La Thuile 2007 FLUXNET data set (Agarwal et al., 2010). Annual files for each site ("site years") that recorded K_G, PAR, and PAR_D in 30 min increments were initially selected, and K_{Ex} was modeled for each 30 min period using the method described in Oliphant et al. (2003). τ was subsequently derived using equation (2). Quality assurance tests for data from each site year was then conducted using plausible bounds testing for each of the key measured variables, as well as tests on ϕ/τ to remove unrepresentative PAR_D values that can arise from a misaligned shade ring or off-level sensor site years with more than 1,000 quality-assured daytime ($\beta > 5°$) 30 min periods were included in further analysis. This includes the 58 sites listed in Table 2 and mapped in Figure 1, providing a total of 140 site years. The data span latitudes from 15°S to 69°N, an elevation range from −6 to 1,770 m above sea level, and include both continental and coastal/island locations as well as locations within and distant from urban areas.

2.4. Analytical Methods

First, ϕ and PAR_D were modeled for each daytime 30 min period of each site year using each of the four models outlined above, all driven by τ which was derived independently for each period at each site. Modeled ϕ was then compared to independently observed ϕ for all available 30 min periods for each site year. Standard descriptive statistics were produced for each site year including root mean square error, coefficient of determination (r^2), and the slope and intercept of linear relationships. In addition, the Nash and Sutcliffe (1970) modeling efficiency coefficient (MEC) was calculated to assess the predictive power of the model:

$$\text{MEC} = 1 - \frac{\sum_{t=1}^{T}\left(\phi_o^t - \phi_m^t\right)^2}{\sum_{t=1}^{T}\left(\phi_o^t - \overline{\phi_o}\right)^2}, \tag{17}$$

where subscripts o and m refer to observational and modeled data respectively, t is the time period (here 30 min), T is the time period of the full record, and the overbar represents the site year average. We then explore the relationship between the residuals of the model identified as superior based on the MEC and latitude, solar zenith angle, air temperature, and humidity following Reindl et al. (1990) and use the FLUXNET data set to explore if near-surface observations can be used to further improve universal application of radiation partitioning models.

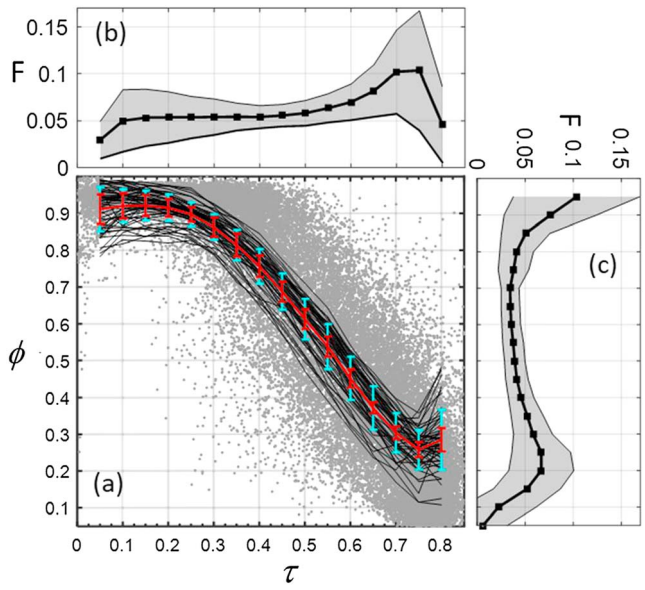

Figure 2. Relationship between and distributions of atmospheric transmissivity (τ) and diffuse photosynthetically active radiation fraction (ϕ) for all sites, including (a) 0.05-wide bin averages of τ for each site (thin black lines) with their average ±1 standard deviation error bars (red lines) as well as the average standard deviation for the individual sites (cyan error bars). These overlay 3 years of 30 min data from a single site (Morgan-Monroe State Forest: gray dots). The frequency (F) distributions represent the 0.05-width bins of (b) τ and (c) ϕ, including all-site average for each bin (thick line with black markers) ±1 standard deviation (shaded area).

3. Results

3.1. Relationship Between τ and ϕ

The negative relationship between τ and ϕ that is described by the four diffuse partitioning models is evident in all 58 sites, as well as two inflection points occurring at τ values of approximately 0.25 and 0.75 (Figure 2). The distribution of both ϕ and τ is bimodal among the sites, with the low τ mode coupled with the high ϕ mode and vice versa. Oliphant et al. (2011) showed for a single site using ceilometer data that these modes generally reflect cloud-free and cloudy periods, respectively, with relatively little

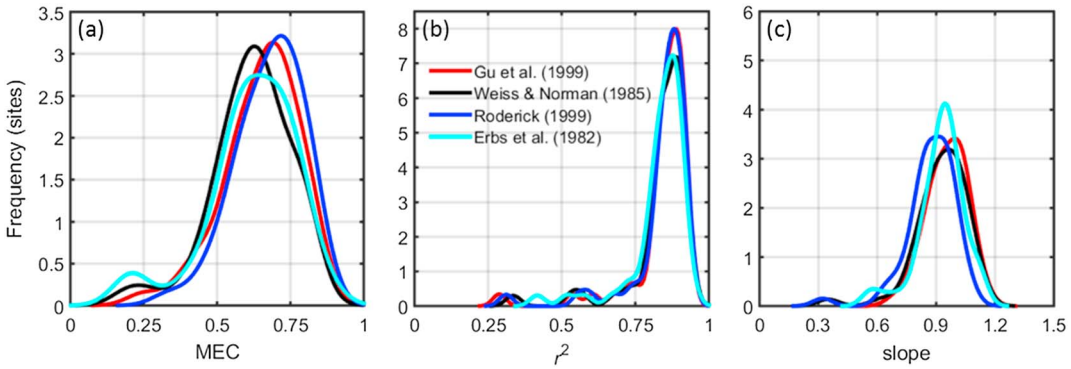

Figure 3. Frequency distributions of model statistics from all sites, including (a) model efficiency coefficient (MEC), (b) coefficient of determination, and (c) slope of the linear regression.

overlap. Therefore, the large range in cloud-free ϕ values is driven predominantly by variability in aerosol concentration and size distribution, as well as atmospheric path length. The largest intersite variability in both ϕ and τ occurs near the two modes, indicating differences in cloud frequency between the sites included.

The variability of ϕ for a given level of τ across sites was relatively low (standard deviation (SD) = 0.061) but tended toward higher variability under clearer skies. The intrasite variability was smaller on average (SD = 0.033) and also quite consistent but tended toward lower variability under clearer skies. In particular, a fairly wide range of low τ values ($0 < \phi < 0.4$) produces a narrow range of high ϕ values ($0.85 < \phi < 1.0$) and yet a narrow range of high τ ($0.65 < \tau < 0.75$) values can produce a relatively wide range of low ϕ values ($0.1 < \phi < 0.4$). This suggests that all but the most optically thin clouds tend to produce high levels of PAR scattering (ϕ = 0.9–0.95) and that under "clear" skies, aerosols have a much smaller impact on τ than ϕ. A simple empirical model derived from this relationship and applied at the 30 min timescale will therefore be more accurate at the site level under clear-sky than cloudy conditions. A universal model on the other hand will tend to be more accurate under cloudy conditions and will be more accurate when applied to cloudier locations.

3.2. Model Performance

The diffuse fraction of PAR was modeled for each 30 min period of each site year when quality-assured K_G was available as a model input. Modeled ϕ values were then compared to observed ϕ for all periods when quality-assured PAR and PAR_D were available. The site distributions of comparative statistics and slope coefficients of the linear fit between modeled and observed ϕ are presented in Figure 3 and their median values provided in Table 3. All four models produce ϕ values that are similarly and closely correlated with observations. The similar goodness of fit values among models probably reflects the similarity in the models in representing the basic relationship described in Figure 2a. The differences between the slope and MEC on the other hand reflect differences in the description of this relationship by each of the models across sites. Based on MEC as the best overall descriptor of model performance, the Roderick (1999) (0.69) and Gu et al. (1999) (0.67) approaches appear to perform slightly better than the other two (both 0.62).

The model residuals were investigated with respect to basic geographic and near-surface atmospheric characteristics that might shed light on model performance: latitude, elevation, solar zenith angle, and, following Reindl et al. (1990), near-surface temperature and RH. Latitude and elevation were not related to any goodness of fit statistic explored here, but solar zenith angle, temperature, and RH are related to model residuals for at least one of the models (Figure 4 and Table 4). Correlation values with these variables are mostly quite weak when considering all sites (with one exception, all correlations lie within $-0.046 < r < 0.084$). The major exception is the Erbs et al. (1982) model, which produces errors negatively correlated with temperature and positively correlated with solar zenith angle (which themselves

Table 3
Median Values of Goodness of Fit Statistics for Different Radiation Partitioning Models, MEC = Model Efficiency Coefficient and R^2 = Coefficient of Determination

Variable	Gu et al. (1999)	Weiss and Norman (1985)	Roderick (1999)	Erbs et al. (1982)
MEC	0.67	0.62	0.69	0.62
R^2	0.87	0.87	0.87	0.85
Slope	0.95	0.94	0.89	0.93

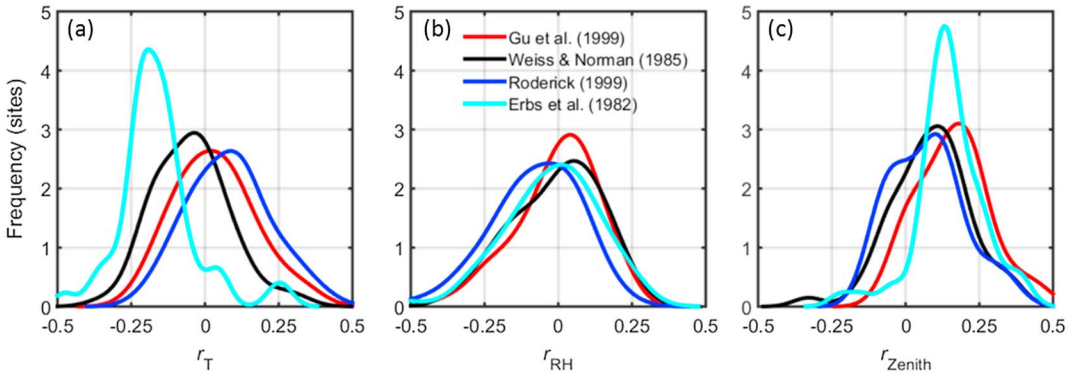

Figure 4. Distribution of correlation coefficients (*r*) between model residuals and environmental variables for all sites including (a) air temperature, (b) relative humidity, and (c) solar zenith angle.

are highly anticorrelated), and the Gu et al. (1999) model, which tends to be positively correlated with solar zenith angle.

Frequency distributions of modeled ϕ at each site were compiled and compared to observed distributions (Figure 5). All four models tended to overestimate frequency distributions of ϕ values in the region of the two modes (approximately $\phi < 0.3$ and $\phi > 0.9$) and to underestimate values in the range between (0.3 and 0.9). The largest underestimation tends to occur in the regions bordering the two modes. Though it generally followed the pattern of the other models, the overestimation of the frequency distributions around the modes is lower for the Roderick (1999) model, and it is the only model where the predicted distribution is fully within one standard deviation of the observed distributions. In particular, this model accurately predicted frequency distributions at intermediate levels of ϕ, with frequency differences in this range generally less than 2%.

4. Discussion

The quality of modeling ϕ using the relationship between τ and ϕ is reliant on the consistency of the relationship between the two atmospheric variables, both between sites and over time at a given site. Given the differences in the relationship between τ and ϕ under different sky conditions and difference in the climatology of cloud and aerosols between sites, there is a limit to the accuracy of a universally applied model to partition PAR_D and PAR_S from PAR. On the other hand, given the reasonable results achieved by all models, the universal applicability with no a priori knowledge of sky conditions and the widespread availability of solar radiation measurements, there is significant value in semiempirical models for partitioning PAR. Our analyses of the comparative statistics and frequency distributions of the four commonly used models suggests that the Roderick (1999) and Gu et al. (1999) models performed better in partitioning PAR than the other two overall. In the following discussion, we use the FLUXNET La Thuille data set to further explore two key features of the model: the optimization of location of the two inflection points for global application and the shape of the negative relationship between them (Figure 2a).

4.1. Optimizing the Inflection Points and Shape of the Diffuse Fraction Model

Although all four models are driven by empirical evidence of the basic form of the relationship described in Figure 2a, much of the difference between the four models can be attributed to different locations of the two

Table 4
The Median Correlation Coefficient ±1 Standard Deviation Between Environmental and Orbital Variables and Model Residuals

Variable	Gu et al. (1999)	Weiss and Norman (1985)	Roderick (1999)	Erbs et al. (1982)
Temperature	0.039 ± 0.13	−0.046 ± 0.13	0.081 ± 0.14	−0.16 ± 0.13
Relative humidity	0.001 ± 0.14	−0.011 ± 0.14	−0.084 ± 0.14	−0.037 ± 0.15
Zenith	0.16 ± 0.12	0.081 ± 0.13	0.069 ± 0.12	0.15 ± 0.12

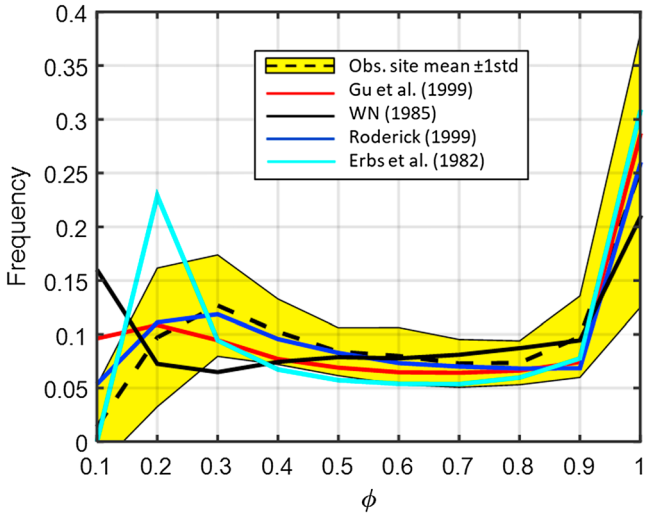

Figure 5. Frequency of 30 min periods for each 0.1 bin of ϕ, including observed site mean and standard deviation, as well as site mean frequencies based on simulations of each of the four models for each site. The frequencies plotted indicate the bin (0.1 width) preceding each *x* axis value.

inflection points and thus the slope of the negative relationship. The inflection point at the upper bound of ϕ can be defined by τ_0, ϕ_0 and the lower inflection point by τ_1, ϕ_1. Based on the locations of the two inflection points given by Alton (2008), Erbs et al. (1982), and Roderick (1999) and confirmed by evidence in Figure 2, a 21 × 21 array of possible inflection point locations was created. The dimensions of the inflections point arrays were (0.1–0.5(τ_0)), (0.6–1.0(ϕ_0)) and (0.6–1.0(τ_1)), (0–0.4(ϕ_1)) and the resolution in both dimensions was 0.02. Since previous models agreed more closely on the location of the first inflection point (τ_0, ϕ_0) relative to the second, we first fixed the initial inflection point to the values supplied by Roderick (1999), τ_0 = 0.26, ϕ_0 = 0.96, and simulated ϕ for each possible location of the second inflection point. The point in the array (τ_1, ϕ_1) that produced the highest MEC was then fixed and the same process was run on the first inflection point (τ_0, ϕ_0). Further iterations were conducted to ensure stability of optimal inflection point location. The MEC for all possible locations in the arrays for each of the two inflection points is displayed for the Morgan-Monroe State Forest, USA (MMSF) site (Figure 6). The optimum inflection points for the case of MMSF were τ_0 = 0.26, ϕ_0 = 0.95, τ_1 = 0.78, ϕ_1 = 0.22, with a MEC of 0.84.

In addition, the shape of the response between the inflection points can be modified from a straight line (equation (13)) by

$$\text{for} \tau_0 < \tau < \tau_1, \quad \phi = \emptyset_0 - (\emptyset_0 - \emptyset_1)\tau_a{}^x, \tag{18}$$

where τ_a is an adjustment to τ that sets the region $\tau_0 < \tau < \tau_1$ to be between 0 and 1 by

$$\tau_a = \frac{(\tau - \tau_0)}{(\tau_1 - \tau_0)}, \tag{19}$$

and *x* is an exponent that can vary to produce a range of curvatures to describe the relationship between the inflection points (Figure 6). A sensitivity analysis of *x* was conducted, and optimal *x* was identified by the *x* value that produced the highest MEC. For MMSF, optimal *x* was found to be 1.0 (a straight line), suggesting that the relationship between τ and ϕ is linear, at least between site-optimized inflection points.

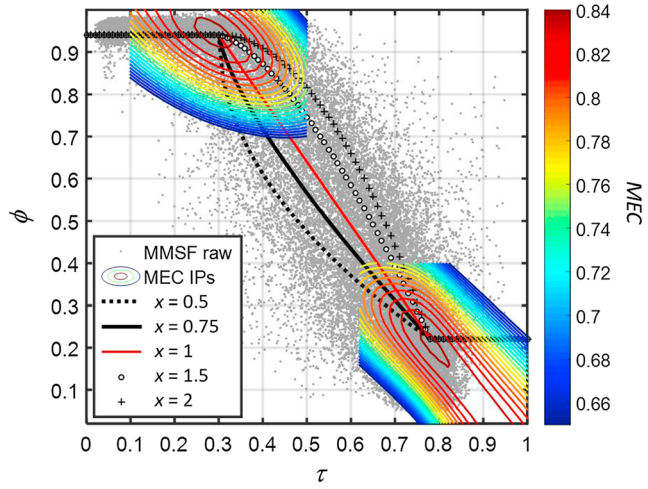

Figure 6. Relationship between ϕ and τ for 3 years of 30 min data from Morgan-Monroe State Forest (MMSF) with the results of inflection point optimization for that site. The contour lines represent the strength of model efficiency coefficient (MEC) results from within the arrays tested for each inflection point (IP). The curved lines between the inflection points represent a range of curvature models applied to the optimal site inflection points, with *x* being the coefficient described in equation (18).

Simulations of ϕ were then conducted for each site as described above and both optimum inflection points were calculated. Figure 7 shows the optimal inflection points from the site level analysis (for *x* = 1). The optimal inflection points are quite narrowly clustered, though more so in the τ than the ϕ dimensions. The outliers in each cluster are dominated by sites with MEC values less than 0.5. The inflection point dimensions are fairly normally distributed, and the median, mode, and mean were all quite close (Table 5). The central tendency of optimal inflection points were identified by the site median inflection points, so as to avoid the influence of outliers and slight skewness of the distribution. The resulting modified universal inflection points are different from the previous models (Gu et al., 1999; Roderick, 1999), particularly, in that ϕ_1 is higher and τ_1 lower in the current analysis.

Each of the four model coefficients that define the two inflection points were tested against annual average temperature, RH and friction velocity, annual total precipitation, and latitude. These did not yield significant or consistent correlations ($r^2 < 0.05$), with one

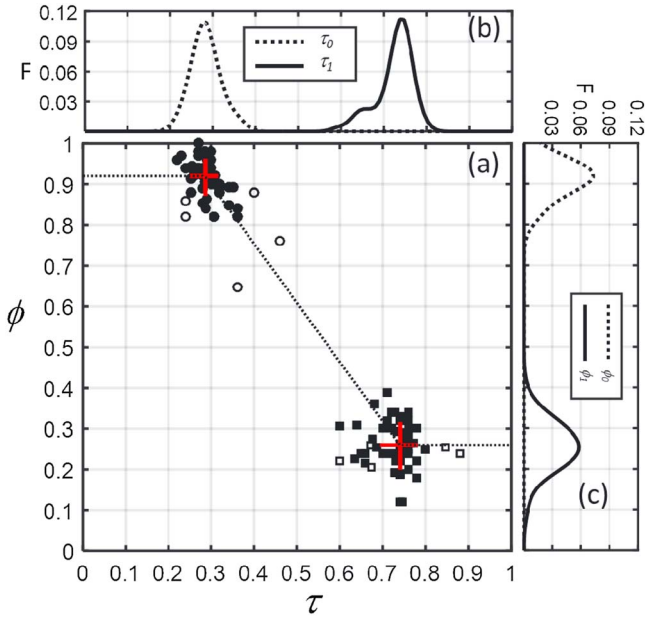

Figure 7. (a) Optimal inflection points determined from 58 sites, where the solid markers show site where model efficiency coefficient > 0.5, as well as median ±1 standard deviation of optimal inflection points from sites where model efficiency coefficient > 0.5 (red crosses). (b) and (c) show the frequency (*F*) distributions of each variable at each inflection point.

exception, the effect of annual mean RH on ϕ_1 (r^2 = 0.21). The resulting linear adjustment to this coefficient is

$$\phi_1 = 0.0044\ \mathrm{RH} - 0.078 \quad (20)$$

The mean optimum *x* across different study sites calculated following the optimization of $\phi_{1,2}$ and $\tau_{1,2}$ was 1.028, with relatively little variation (SD = 0.056) (Figure 8). This suggests that the linear form is appropriate if effective inflection points are used. When *x* was tested for all sites using the new universal optimal inflection points (median values from Table 5), the mean optimum *x* did not change (1.027), but the variation between sites became larger (SD = 0.296). This suggests that site-optimized *x* was offsetting some of the errors associated with non-site-optimal inflection point locations but that ϕ still tends to respond linearly overall to τ between the inflection points.

The comparison of MEC between the current and previous universal models as well as site-specific variants shows that the universal inflection points found here generally perform better than previous models for this data set, with site median MEC values increasing from 0.67 to 0.73 (Figure 9). Using RH to determine ϕ_1 (equation (20)) made a visible improvement to the MEC distribution, but the site median MEC only improved from 0.7265 to 0.7293. Unsurprisingly, site-specific inflection points perform better than any universal function (site median MEC = 0.78). The lack of correlation between inflection point locations and latitude, temperature, or humidity suggests that differences in inflection point locations are likely governed primarily by differences in sky conditions rather than astronomical patterns. This means using site or nearby-derived optimal inflection points where possible is recommended. The fact that optimal *x* was close to 1 for both site-specific and universal inflection points means universal *x* adjustment is not warranted. A site-specific *x* can improve model performance using universal inflection points, but this is just helping offset error generated by the universal function. Finding the optimum inflection points produces considerably better results and makes shape adjustments unnecessary.

4.2. Implications for Biogeoscience Studies

Semiempirical models of the diffuse fraction of PAR with limited a priori knowledge have been widely used over the past several decades to drive ecosystem photosynthesis and carbon cycle models. These are used for prognostic or diagnostic modeling objectives, as well as gap-filling observational records across space or time. Recent results by Lee et al. (2018) have reiterated the importance of improving models of PAR_D for modeling gross primary productivity (GPP) at the annual scale and noted that interannual variation in PAR_D was important for describing the interannual variability of eddy covariance-estimated GPP, which continues to elude ecosystem models (Niu et al., 2017). Investigation of the residuals for an individual site indicates that errors are by far the largest in the middle range of ϕ (as evidenced in Figure 2a). In general, we found that this led to an underestimation of the amount of time these conditions existed (Figure 5). Although this middle range of values is also relatively infrequent in occurrence at most sites compared with the two modes (Figure 2c), ϕ values in this range have been shown to produce the highest light use efficiencies for plant photosynthesis (Alton, 2008; Oliphant et al., 2011; Pedruzo-Bagazgoitia et al., 2017). GPP models based on diffuse beam partitioning models will therefore likely underestimate observed GPP based on errors in the diffuse partitioning, as found by Lee et al. (2018).

Improvement in PAR_D estimates will also propagate to modeling energy budgets of plant canopies or ecosystems in complex terrain, since the diffuse beam incident angle is much closer to isotropic in

Table 5
Statistical Results of the Distribution of Optimal Inflection Points for the 52/58 Sites in Which the Model Efficiency Coefficient (MEC) Was Greater Than 0.5

Statistic	τ_0	τ_1	ϕ_0	ϕ_1
Mean	0.294	0.730	0.904	0.259
Median	0.286	0.740	0.920	0.260
Mode	0.284	0.740	0.917	0.246
Standard deviation	0.031	0.042	0.043	0.056

Note. Abbreviations found in Table 1.

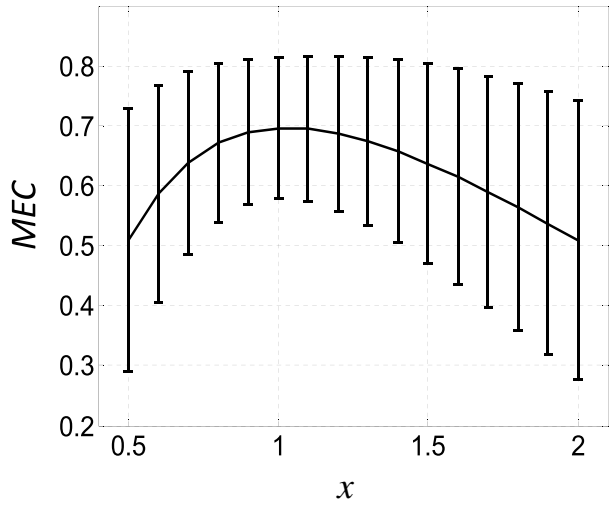

Figure 8. Average and standard deviation model efficiency coefficient (MEC) values for varying levels of x applied to 58 sites.

incident angle and therefore produces much greater spatial homogeneity of canopy irradiance. Inaccuracies in partitioning modeling will therefore tend to underestimate the midclear conditions when relatively high levels of light coincide with significant scattering. In these conditions some of the highest incident light occurs in locations normally shaded from the direct beam.

The results of this study provide a modest improvement to universal diffuse fraction models, and a method to improve accuracy further through optimization of model coefficients at the site level. These in turn should provide modest improvements to a range of biophysical models, including for annual estimates of GPP (Lee et al., 2018). However, we found that the model could not be further improved significantly using latitude or commonly measured climate variables. Due to the variability in the relationship between τ and ϕ evident in observational records even at the individual site year level, this probably reflects an upper limit to accuracy to this approach for a model that is universal in space and time. Given the lack of latitudinal, or climate correlation with model coefficients, this variability is likely to be driven by changes over time in type and depth of clouds, and concentrations of aerosols of different size distributions and locations within the atmospheric column. Although this information is difficult to obtain, models that incorporate observations of the atmosphere from remote sensing or other measurements may lead to greater spatiotemporal accuracy in modeling PAR_D. This also suggests that additional accuracy may be obtained from regional optimization of model coefficients, or from seasonal optimization at the site level. For individual sites, significant accuracy gains can be made from site optimization of model coefficients and for photosynthesis process studies, it may also improve accuracy to generate model coefficients using only growing season data. For reference, the full table of optimal model coefficients and statistics for each of the 58 sites, as well as code for implementation of the model formatted as a Matlab function, are provided in the supporting information. Ultimately, accuracy limitations of all models evaluated and the importance of diffuse light to ecosystem productivity suggest the usefulness of flux tower sites including accurate measurements of diffuse PAR.

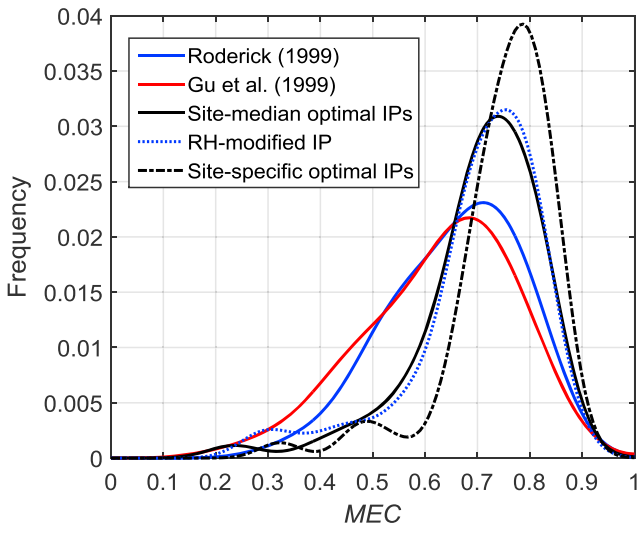

Figure 9. Frequency distribution of model efficiency coefficient (MEC) for model ensembles using 58 sites, including results from different models derived here and those from previous models, where IPs refers to the inflection points in the model and RH-modified IP refers to the model that uses annual mean relative humidity to modify ϕ_1.

5. Conclusions

We investigated a global data set of solar radiation and photosynthetically active radiation observations at 58 sites (140 site years) in the FLUXNET La Thuille database to examine and improve semiempirical models that partition PAR into diffuse and direct beam components using global solar radiation as input. We tested the ability of four existing models (Erbs et al., 1982; Gu et al., 1999; Roderick, 1999; Weiss & Norman, 1985) to predict the diffuse beam fraction of PAR (ϕ) at the 30 min timescale. The four models predicted ϕ with site median r^2 values ranging between 0.85 and 0.87 and model efficiency coefficients between 0.62 and 0.69. All models tended to overpredict the frequency of low and high ϕ values and underpredict midlevel ϕ values. Model residuals at the 30 min timescale were not strongly correlated with astronomical or standard meteorological variables, with the greatest exception being Erbs et al. (1982), which was negatively correlated with temperature ($r = -0.17$). From comparative statistics as well as examination of the modeled distributions and residuals, we conclude that the Roderick (1999) and Gu et al. (1999) models performed better overall than the two older variants.

The general model form described by existing models is a simple nonlinear relationship between solar transmissivity (τ) and ϕ, with two

inflection points at high and low ϕ levels and a linear negative relationship between the two inflection points. We used the data set to optimize the locations of the two inflection points as well as the curvature of the relationship between the inflection points. For each site, statistically optimal (maximum MEC) inflection point locations were found and optimal curvature in the line between the points. Optimizing inflection points for each site made a significant improvement to the model as expected due to the site-specific training, with site median MECs increasing from 0.67 for the existing models to 0.78. The median optimal curvature coefficient on the other hand was found to be 1.028 with very little variability, meaning the optimal modeled relationship between the inflection points was near linear at all sites. The site median optimal inflection points, when applied as a universal function across the data set improved model performance significantly with MEC increasing from 0.67 to 0.73. The model coefficients were tested against standard site climate information and weak to no correlation was found except for site annual mean RH, which explained about 20% of the variability of one of the coefficients. However, when included in the universal model, it raised site median MEC by only 0.0028. This new universal function has four coefficients that determine the coordinates of the two inflection points and can be applied as follows (Matlab code provided in the supporting information);

$$\text{for}\tau < \tau_0; \phi = \phi_0 \quad \text{for}\tau_0 < \tau < \tau_1; \quad \phi = A_0 + A_1\tau, \quad \text{and for}\tau > \tau_1; \phi = \phi_1 \tag{21}$$

$$\text{where } A_1 = \frac{\phi_1 - \phi_0}{\tau_1 - \tau_0} \text{ and } A_0 = \phi_1 - A_1\tau_1, \tag{22}$$

where the model coefficients that define the optimal inflection point coordinates are $\tau_0 = 0.286$, $\phi_0 = 0.92$, $\tau_1 = 0.74$, and $\phi_1 = 0.26$.

Acknowledgments

This work used data acquired by the FLUXNET community and in particular by the following networks: AmeriFlux (U.S. Department of Energy, Biological and Environmental Research, Terrestrial Carbon Program (DE-FG02-04ER63917 and DE-FG02-04ER63911)), AsiaFlux, CarboEuropeIP, CarboItaly, ChinaFlux, and OzFlux. We acknowledge the financial support to the database development and technical support from Berkeley Water Center, Lawrence Berkeley National Laboratory, Microsoft Research eScience, Oak Ridge National Laboratory, University of California-Berkeley, and University of Virginia (data source: http://fluxnet.fluxdata.org/data/la-thuile-dataset/). In particular, the authors are indebted to the researchers and staff associated with the sites used in this study (Table 2) as well as to past and present researchers and staff of the Morgan Monroe State Forest eddy flux site, whose data informed the initial basis of this work. In addition, A. J. O. had funding support from the U.S. National Science Foundation's Geographical and Spatial Sciences Program 19002200 and P. C. S. acknowledges funding support from the U.S. National Science Foundation Division of Environmental Biology grant 1552976 and the U.S. Department of Agriculture Hatch Project 228396.

References

Agarwal, D. A., Humphrey, M., Beekwilder, N. F., Jackson, K. R., Goode, M. M., & van Ingen, C. (2010). A data-centered collaboration portal to support global carbon-flux analysis. *Control and Computer Practice Experimental*, *22*(17), 2323–2334. https://doi.org/10.1002/cpe.1600

Alados, I., Foyo-Moreno, I., Olmo, F. J., & Alados-Arboledas, L. (2002). Improved estimation of diffuse photosynthetically active radiation using two spectral models. *Agricultural and Forest Meteorology*, *111*(1), 1–12. https://doi.org/10.1016/S0168-1923(02)00010-2

Alton, P. B. (2008). Reduced carbon sequestration in terrestrial ecosystems under overcast skies compared to clear skies. *Agricultural and Forest Meteorology*, *148*(10), 1641–1653. https://doi.org/10.1016/j.agrformet.2008.05.014

Anthoni, P. M., Knohl, A., Rebmann, C., Freibauer, A., Mund, M., & Ziegler, W. (2004). Forest and agricultural land-use-dependent CO_2 exchange in Thuringia, Germany. *Global Change Biology*, *10*(12), 2005–2019. https://doi.org/10.1111/j.1365-2486.2004.00863.x

Anthoni, P. M., Freibauer, A., Kolle, O., & Schulze, E.-D. (2004). Winter wheat carbon exchange in Thuringia, Germany. *Agricultural and Forest Meteorology*, *121*(1), 55–67.

Aubinet, M., Chermanne, B., Vandenhaute, M., Longdoz, B., Yernaux, M., & Laitat, E. (2001). Long term carbon dioxide exchange above a mixed forest in the Belgian Ardennes. *Agricultural and Forest Meteorology*, *108*(4), 293–315. https://doi.org/10.1016/S0168-1923(01)00244-1

Aurela, M., Laurila, T., & Tuovinen, J. P. (2002). Annual CO_2 balance of a subarctic fen in northern Europe: Importance of the wintertime efflux. *Journal of Geophysical Research*, *107*(D21), 4607. https://doi.org/10.1029/2002JD002055

Baldocchi, D., Falge, E., Gu, L., Olsen, R., Hollinger, D., Running, S., et al. (2001). FLUXNET: A new tool to study the temporal and spatial variability of ecosystem-scale carbon dioxide, water vapor, and energy flux densities. *Bulletin of the American Meteorological Society*, *82*(11), 2415–2434. https://doi.org/10.1175/1520-0477(2001)082%3C2415:FANTTS%3E2.3.CO;2

Berbigier, P., Bonnefond, J.-M., & Mellmann, P. (2001). CO_2 and water vapour fluxes for 2 years above Euroflux forest site. *Agricultural and Forest Meteorology*, *108*(3), 183–197. https://doi.org/10.1016/S0168-1923(01)00240-4

Bernhofer, C., Aubinet, M., Clement, R., Grelle, A., Grünwald, T., Ibrom, A., et al. (2003). Spruce forests (Norway and Sitka spruce, including Douglas fir): Carbon and water fluxes and balances, ecological and ecophysiological determinants. In *Fluxes of carbon, water and energy of European forests* (pp. 99–123). Berlin: Springer-Verlag.

Béziat, P., Ceschia, E., & Dedieu, G. (2009). Carbon balance of a three crop succession over two cropland sites in South West France. *Agricultural and Forest Meteorology*, *149*(10), 1628–1645. https://doi.org/10.1016/j.agrformet.2009.05.004

Black, K., Davis, P., Lynch, P., Jones, M., McGettigan, M., & Osborne, B. (2006). Long-term trends in solar irradiance in Ireland and their potential effects on gross primary productivity. *Agricultural and Forest Meteorology*, *141*(2), 118–132.

Carvalhais, N., Reichstein, M., Collatz, G. J., Mahecha, M. D., Migliavacca, M., Neigh, C. S. R., et al. (2010). Deciphering the components of regional net ecosystem fluxes following a bottom-up approach for the Iberian Peninsula. *Biogeosciences*, *7*, 3707–3729.

Cescatti, A., & Marcolla, B. (2004). Drag coefficient and turbulence intensity in conifer canopies. *Agricultural and Forest Meteorology*, *121*(3-4), 197–206. https://doi.org/10.1016/j.agrformet.2003.08.028

Cheng, S. J., Bohrer, G., Steiner, A. L., Hollinger, D. Y., Suyker, A., Phillips, R. P., & Nadelhoffer, K. J. (2015). Variations in the influence of diffuse light on gross primary productivity in temperate ecosystems. *Agricultural and Forest Meteorology*, *201*, 98–110. https://doi.org/10.1016/j.agrformet.2014.11.002

Cheng, S. J., Steiner, A. L., Hollinger, D. Y., Bohrer, G., & Nadelhoffer, K. J. (2016). Using satellite-derived optical thickness to assess the influence of clouds on terrestrial carbon uptake. *Journal of Geophysical Research: Biogeosciences*, *121*, 1747–1761. https://doi.org/10.1002/2016JG003365

Chiesi, M., Maselli, F., Bindi, M., Fibbi, L., Cherubini, P., Arlotta, E., et al. (2005). Modelling carbon budget of Mediterranean forests using ground and remote sensing measurements. *Agricultural and Forest Meteorology*, *135*(1-4), 22–34. https://doi.org/10.1016/j.agrformet.2005.09.011

Chojnicki, B. H., Urbaniak, M., Józefczyk, D., Augustin, J., & Olejnik, J. (2007). Measurements of gas and heat fluxes at Rzecin wetland. In T. Okrus, et al. (Eds.), *Wetlands: Monitoring, modelling and management* (pp. 125–131). London: Taylor & Francis.

Cook, B. D., Davis, K. J., Wang, W., Desai, A., Berger, B. W., Teclaw, R. M., et al. (2004). Carbon exchange and venting anomalies in an upland deciduous forest in northern Wisconsin, USA. *Agricultural and Forest Meteorology*, *126*(3-4), 271–295. https://doi.org/10.1016/j.agrformet.2004.06.008

Davi, H., Dufrêne, E., Francois, C., Le Maire, G., Loustau, D., Bosc, A., et al. (2006). Sensitivity of water and carbon fluxes to climate changes from 1960 to 2100 in European forest ecosystems, *Agricultural and Forest Meteorology*, *141*(1), 35–56. https://doi.org/10.1016/j.agrformet.2006.09.003

de Pury, D. G. G., & Ceulemans, R. (1997). Scaling-up carbon fluxes from leaves to stands in a patchy coniferous/deciduous Forest. In *Impacts of global change on tree physiology and forest ecosystems* (pp. 263–272). Dordrecht, Netherlands: Springer.

Dolman, A. J., Moors, E. J., & Elbers, J. A. (2002). The carbon uptake of a midlatitude pine forest growing on sandy soil. *Agricultural and Forest Meteorology*, *111*(3), 157–170. https://doi.org/10.1016/S0168-1923(02)00024-2

Don, A., Rebmann, C., Kolle, O., Scherer-Lorenzen, M., & Schulze, E.-D. (2009). Impact of afforestation-associated management changes on the carbon balance of grassland. *Global Change Biology*, *15*(8), 1990–2002. https://doi.org/10.1111/j.1365-2486.2009.01873.x

Erbs, D. G., Klein, S. A., & Duffie, J. A. (1982). Estimation of the diffuse radiation fraction for hourly, daily and monthly-average global radiation. *Solar Energy*, *28*, 293–302.

Famulari, D., Fowler, D., Hargreaves, K., Milford, C., Nemitz, E., Sutton, M. A., & Weston, K. (2004). Measuring eddy covariance fluxes of ammonia using tunable diode laser absorption spectroscopy. *Water, Air, & Soil Pollution: Focus*, *4*(6), 151–158.

Gilmanov, T. G., Soussana, J. F., Aires, L., Allard, V., Ammann, C., Balzarolo, M., et al. (2007). Partitioning European grassland net ecosystem CO_2 exchange into gross primary productivity and ecosystem respiration using light response function analysis. *Agriculture, Ecosystems and Environment*, *121*(1-2), 93–120. https://doi.org/10.1016/j.agee.2006.12.008

Goudriaan, J., & Van Laar, H. H. (2012). *Modelling potential crop growth processes: Textbook with exercises*. Berlin: Springer Science & Business Media.

Granier, A., Ceschia, E., Damesin, C., Dufrêne, E., Epron, D., Gross, P., et al. (2000). The carbon balance of a young beech forest. *Functional Ecology*, *14*(3), 312–325. https://doi.org/10.1046/j.1365-2435.2000.00434.x

Gu, L. H., Fuentes, J. D., Shugart, H. H., Staebler, R. M., & Black, T. A. (1999). Responses of net ecosystem exchanges of carbon dioxide to changes in cloudiness: Results from two North American deciduous forests. *Journal of Geophysical Research*, *104*(D24), 31,421–31,434. https://doi.org/10.1029/1999JD901068

Gu, L. H., Baldocchi, D., Verma, S. B., Black, T. A., Vesala, T., Falge, E. M., & Dowty, P. R. (2002). Advantages of diffuse radiation for terrestrial ecosystem productivity. *Journal of Geophysical Research*, *107*(D6), 4050.

Hutley, L. B., O'grady, A. P., & Eamus, D. (2000). Evapotranspiration from Eucalypt open-forest savanna of Northern Australia. *Functional Ecology*, *14*(2), 183–194. https://doi.org/10.1046/j.1365-2435.2000.00416.x

Keppel-Aleks, G., & Washenfelder, R. A. (2016). The effect of atmospheric sulfate reductions on diffuse radiation and photosynthesis in the United States during 1995–2013. *Geophysical Research Letters*, *43*, 9984–9993. https://doi.org/10.1002/2016GL070052

Knohl, A., Schulze, E.-D., Kolle, O., & Buchmann, N. (2003). Large carbon uptake by an unmanaged 250-year-old deciduous forest in Central Germany. *Agricultural and Forest Meteorology*, *118*(3-4), 151–167. https://doi.org/10.1016/S0168-1923(03)00115-1

Lagergren, F., Eklundh, L., Grelle, A., Lundblad, M., Mölder, M., Lankreijer, H., & Lindroth, A. (2005). Net primary production and light use efficiency in a mixed coniferous forest in Sweden. *Plant, Cell & Environment*, *28*(3), 412–423. https://doi.org/10.1111/j.1365-3040.2004.01280.x

Laville, P., Jambert, C., Cellier, P., & Delmas, R. (1999). Nitrous oxide fluxes from a fertilised maize crop using micrometeorological and chamber methods. *Agricultural and Forest Meteorology*, *96*(1-3), 19–38. https://doi.org/10.1016/S0168-1923(99)00054-4

Law, B. E., Goldstein, A. H., Anthoni, P. M., Unsworth, M. H., Panek, J. A., Bauer, M. R., et al. (2001). Carbon dioxide and water vapor exchange by young and old ponderosa pine ecosystems during a dry summer. *Tree Physiology*, *21*(5), 299–308. https://doi.org/10.1093/treephys/21.5.299

Lee, M., Hollinger, D. Y., Keenan, T., Ouimette, A. P., Ollinger, S. V., & Richardson, A. D. (2018). Model-based analysis of the impact of diffuse radiation on CO2 exchange in a temperate deciduous forest. *Agricultural and Forest Meteorology*, *249*, 377–389. https://doi.org/10.1016/j.agrformet.2017.11.016

Leuning, R., Kelliher, F. M., DePury, D. G., & Schulze, E.-D. (1995). Leaf nitrogen, photosynthesis, conductance and transpiration: Scaling from leaves to canopies. *Plant, Cell and Environment*, *18*(10), 1183–1200. https://doi.org/10.1111/j.1365-3040.1995.tb00628.x

Lindberg, F., Holmer, B., Thorsson, S., & Raynor, D. (2014). Characteristics of the mean radiant temperature in high latitude cities—Implications for sensitive climate planning applications. *International Journal of Biometeorology*, *58*(5), 613–627. https://doi.org/10.1007/s00484-013-0638-y

Liu, B. Y. H., & Jordan, R. C. (1960). The interrelationship and characteristic distribution of direct, diffuse and total solar radiation. *Solar Energy*, *4*(3), 1–19. https://doi.org/10.1016/0038-092X(60)90062-1

Ma, S., Baldocchi, D. D., Xu, L., & Hehn, T. (2007). Inter-annual variability in carbon dioxide exchange of an oak/grass savanna and open grassland in California. *Agricultural and Forest Meteorology*, *147*(3-4), 157–171. https://doi.org/10.1016/j.agrformet.2007.07.008

Marcolla, B., Cescatti, A., Montagnani, L., Manca, G., Kerschbaumer, G., & Minerbi, S. (2005). Importance of advection in the atmospheric CO_2 exchanges of an alpine forest. *Agricultural and Forest Meteorology*, *130*(3-4), 193–206. https://doi.org/10.1016/j.agrformet.2005.03.006

Marcolla, B., Cescatti, A., Manca, G., Zorer, R., Cavagna, M., Fiora, A., et al. (2011). Climatic controls and ecosystem responses drive the inter-annual variability of the net ecosystem exchange of an alpine meadow. *Agricultural and Forest Meteorology*, *151*(9), 1233–1243. https://doi.org/10.1016/j.agrformet.2011.04.015

Marek, M. V., Janouš, D., Taufarová, K., Havránková, K., Pavelka, M., Kaplan, V., & Marková, I. (2011). Carbon exchange between ecosystems and atmosphere in the Czech Republic is affected by climate factors. *Environmental Pollution*, *159*(5), 1035–1039. https://doi.org/10.1016/j.envpol.2010.11.025

McCartney, E. J. (1976). *Optics of the atmosphere: Scattering by molecules and particles* (Vol. 421, p. 1). New York: John Wiley.

Mercado, L. M., Bellouin, N., Sitch, S., Boucher, O., Huntingford, C., Wild, M., & Cox, P. M. (2009). Impact of changes in diffuse radiation on the global land carbon sink. *Nature*, *458*(7241), 1014–1017. https://doi.org/10.1038/nature07949

Migliavacca, M., Meroni, M., Manca, G., Matteucci, G., Montagnani, L., Grassi, G., et al. (2009). Seasonal and interannual patterns of carbon and water fluxes of a poplar plantation under peculiar eco-climatic conditions. *Agricultural and Forest Meteorology*, *149*(9), 1460–1476. https://doi.org/10.1016/j.agrformet.2009.04.003

Moors, E. J., Jacobs, C., Jans, W., Supit, I., Kutsch, W. L., Bernhofer, C., et al. (2010). Variability in carbon exchange of European croplands. *Agriculture, Ecosystems and Environment*, *139*(3), 325–335. https://doi.org/10.1016/j.agee.2010.04.013

Moureaux, C., Debacq, A., Bodson, B., Heinesch, B., & Aubinet, M. (2006). Annual net ecosystem carbon exchange by a sugar beet crop. *Agricultural and Forest Meteorology*, *139*(1-2), 25–39. https://doi.org/10.1016/j.agrformet.2006.05.009

Nash, J. E., & Sutcliffe, J. V. (1970). River flow forecasting through conceptual models part I—A discussion of principles. *Journal of Hydrology*, *10*(3), 282–290. https://doi.org/10.1016/0022-1694(70)90255-6

Niu, S., Fu, Z., Luo, Y., Stoy, P., Keenan, T. F., Poulter, B., et al. (2017). Interannual variability of ecosystem carbon exchange: From observation to prediction. *Global Ecology and Biogeography*, *26*, 1225–1237. https://doi.org/10.1111/geb.12633

Norman, J. M., & Welles, J. M. (1983). Radiative transfer in an array of canopies. *Agronomy Journal*, *75*(3), 481–488. https://doi.org/10.2134/agronj1983.00021962007500030016x

Nunez, M. (1980). The calculation of solar and net radiation in mountainous terrain. *Journal of Biogeography*, *173–186*.

Oliphant, A. J., Spronken-Smith, R. A., Sturman, A. P., & Owens, I. F. (2003). Spatial variability of surface radiation fluxes in mountainous terrain. *Journal of Applied Meteorology*, *42*(1), 113–128. https://doi.org/10.1175/1520-0450(2003)042%3C0113:SVOSRF%3E2.0.CO;2

Oliphant, A., Grimmond, C. S. B., Schmid, H.-P., & Wayson, C. A. (2006). Local-scale heterogeneity of photosynthetically active radiation (PAR), absorbed PAR and net radiation as a function of topography, sky conditions and leaf area index. *Remote Sensing of Environment*, *103*(3), 324–337. https://doi.org/10.1016/j.rse.2005.09.021

Oliphant, A. J., Dragoni, D., Deng, B., Grimmond, C. S. B., Schmid, H.-P., & Scott, S. L. (2011). The role of sky conditions on gross primary production in a mixed deciduous forest. *Agricultural and Forest Meteorology*, *151*(7), 781–791. https://doi.org/10.1016/j.agrformet.2011.01.005

Pedruzo-Bagazgoitia, X., Ouwersloot, H. G., Sikma, M., van Heerwaarden, C. C., Jacobs, C. M., & Vilà-Guerau de Arellano, J. (2017). Direct and diffuse radiation in the shallow cumulus–vegetation system: Enhanced and decreased evapotranspiration regimes. *Journal of Hydrometeorology*, *18*(6), 1731–1748. https://doi.org/10.1175/JHM-D-16-0279.1

Pereira, J. S., Mateus, J. A., Aires, L. M., Pita, G., Pio, C., David, J. S., et al. (2007). Net ecosystem carbon exchange in three contrasting Mediterranean ecosystems-the effect of drought. *Biogeosciences*, *4*(5), 791–802. https://doi.org/10.5194/bg-4-791-2007

Pilegaard, K., Hummelshøj, P., Jensen, N. O., & Chen, Z. (2001). Two years of continuous CO_2 eddy-flux measurements over a Danish beech forest. *Agricultural and Forest Meteorology*, *107*(1), 29–41. https://doi.org/10.1016/S0168-1923(00)00227-6

Rambal, S., Joffre, R., & Ourcival, J.-M. (2004). The growth respiration component in eddy CO_2 flux from a *Quercus ilex* Mediterranean forest. *Global Change Biology*, *10*(9), 1460–1469. https://doi.org/10.1111/j.1365-2486.2004.00819.x

Reichstein, M., Rey, A., Freibauer, A., Tenhunen, J., Valentini, R., Banza, J., et al. (2003). Modeling temporal and large-scale spatial variability of soil respiration from soil water availability, temperature and vegetation productivity indices. *Global Biogeochemical Cycles*, *17*(4), 1104. https://doi.org/10.1029/2003GB002035

Reindl, D. T., Beckman, W. A., & Duffie, J. A. (1990). Diffuse fraction correlations. *Solar Energy*, *45*(1), 1–7. https://doi.org/10.1016/0038-092X(90)90060-P

Rey, A., Pegoraro, E., & Tedeschi, V. (2002). Annual variation in soil respiration and its components in a coppice oak forest in Central Italy. *Global Change Biology*, *8*(9), 851–866. https://doi.org/10.1046/j.1365-2486.2002.00521.x

Richardson, A. D., Jenkins, J. P., Braswell, B. H., Hollinger, D. Y., Ollinger, S. V., & Smith, M.-L. (2007). Use of digital webcam images to track spring green-up in a deciduous broadleaf forest. *Oecologia*, *152*(2), 323–334. https://doi.org/10.1007/s00442-006-0657-z

Roderick, M. L. (1999). Estimating the diffuse component from daily and monthly measurements of global radiation. *Agricultural and Forest Meteorology*, *95*(3), 169–185. https://doi.org/10.1016/S0168-1923(99)00028-3

Roupsard, O., Bonnefond, J.-M., Irvine, M., Berbigier, P., Nouvellon, Y., Dauzat, J., et al. (2006). Partitioning energy and evapo-transpiration above and below a tropical palm canopy. *Agricultural and Forest Meteorology*, *139*(3-4), 252–268. https://doi.org/10.1016/j.agrformet.2006.07.006

Schmid, H. P., Grimmond, C. S. B., Cropley, F., Offerle, B., & Su, H. B. (2000). Measurements of CO_2 and energy fluxes over a mixed hardwood forest in the mid-western United States. *Agricultural and Forest Meteorology*, *103*(4), 357–374.

Skiba, U., Drewer, J., Tang, Y. S., Van Dijk, N., Helfter, C., Nemitz, E., et al. (2009). Biosphere–atmosphere exchange of reactive nitrogen and greenhouse gases at the NitroEurope core flux measurement sites: Measurement strategy and first data sets. *Agriculture, Ecosystems and Environment*, *133*(3-4), 139–149. https://doi.org/10.1016/j.agee.2009.05.018

Soegaard, H., Jensen, N. O., Boegh, E., Hasager, C. B., Schelde, K., & Thomsen, A. (2003). Carbon dioxide exchange over agricultural landscape using eddy correlation and footprint modelling. *Agricultural and Forest Meteorology*, *114*(3-4), 153–173. https://doi.org/10.1016/S0168-1923(02)00177-6

Soussana, J. F., Allard, V., Pilegaard, K., Ambus, P., Amman, C., Campbell, C., et al. (2007). Full accounting of the greenhouse gas (CO_2, N_2O, CH_4) budget of nine European grassland sites. *Agriculture, Ecosystems and Environment*, *121*(1-2), 121–134. https://doi.org/10.1016/j.agee.2006.12.022

Spitters, C. J. T., Toussaint, H. A. J. M., & Goudriaan, J. (1986). Separating the diffuse and direct component of global radiation and its implications for modeling canopy photosynthesis: Part 1. Components of incoming radiation. *Agricultural and Forest Meteorology*, *38*(1-3), 217–229. https://doi.org/10.1016/0168-1923(86)90060-2

Steiner, A. L., Mermelstein, D., Cheng, S. J., Twine, T. E., & Oliphant, A. J. (2013). Observed impact of atmospheric aerosols on the surface energy budget. *Earth Interactions*, *17*(14), 1–22. https://doi.org/10.1175/2013EI000523.1

Suni, T., Berninger, F., Markkanen, T., Keronen, P., Rannik, U., & Vesala, T. (2003). Interannual variability and timing of growing-season CO_2 exchange in a boreal forest. *Journal of Geophysical Research*, *108*(D9), 4265. https://doi.org/10.1029/2002JD002381

Tedeschi, V., Rey, A. N. A., Manca, G., Valentini, R., Jarvis, P. G., & Borghetti, M. (2006). Soil respiration in a Mediterranean oak forest at different developmental stages after coppicing. *Global Change Biology*, *12*(1), 110–121. https://doi.org/10.1111/j.1365-2486.2005.01081.x

Tirone, G., Dore, S., Matteucci, G., Greco, S., & Valentini, R. (2003). Evergreen Mediterranean forests. Carbon and water fluxes, balances, ecological and ecophysiological determinants. In *Fluxes of carbon, water and energy of European forests* (pp. 125–149). Berlin: Springer.

Valentini, R., de Angelis, P., Matteucci, G., Monaco, R., Dore, S., & Mucnozza, G. E. S. (1996). Seasonal net carbon dioxide exchange of a beech forest with the atmosphere. *Global Change Biology*, *2*(3), 199–207. https://doi.org/10.1111/j.1365-2486.1996.tb00072.x

Verma, S. B., Dobermann, A., Cassman, K. G., Walters, D. T., Knops, J. M., Arkebauer, T. J., et al. (2005). Annual carbon dioxide exchange in irrigated and rainfed maize-based agroecosystems. *Agricultural and Forest Meteorology*, *131*(1-2), 77–96. https://doi.org/10.1016/j.agrformet.2005.05.003

Weiss, A., & Norman, J. M. (1985). Partitioning solar radiation into direct and diffuse, visible and near-infrared components. *Agricultural and Forest Meteorology*, *34*(2-3), 205–213. https://doi.org/10.1016/0168-1923(85)90020-6

Whiteman, C. D., & Allwine, K. J. (1986). Extraterrestrial solar radiation on inclined surfaces. *Environmental Software*, *1*(3), 164–169. https://doi.org/10.1016/0266-9838(86)90020-1

Wohlfahrt, G., Anderson-Dunn, M., Bahn, M., Balzarolo, M., Berninger, F., Campbell, C., et al. (2008). Biotic, abiotic, and management controls on the net ecosystem CO_2 exchange of European mountain grassland ecosystems. *Ecosystems*, *11*(8), 1338–1351. https://doi.org/10.1007/s10021-008-9196-2